Rev. Adv. Mater. Sci. 50 (2017) 104-114

STRESS-DRIVEN SHEAR-COUPLED MIGRATION OF HIGH-ANGLE GRAIN BOUNDARIES IN METAL-GRAPHENE NANOCOMPOSITES

S.V. Bobylev[1,2,3] and I.A. Ovid'ko

[1]Peter the Great St. Petersburg Polytechnic University, St. Petersburg 195251, Russia
[2]St. Petersburg State University, St. Petersburg 199034, Russia
[3]Institute of Problems of Mechanical Engineering, Russian Academy of Sciences, St. Petersburg 199178, Russia

Received: April, 2014

Abstract. A theoretical model is suggested which describes plastic flow through stress-driven shear-coupled migration of high-angle grain boundaries (GBs) in metal-graphene nanocomposites. In the framework of the suggested model, stress-driven shear-coupled GB migration gives rise to the formation of wedge disclinations at GB junctions and edges of graphene inclusions. Energy and stress characteristics of stress-driven shear-coupled GB migration are calculated (in the exemplary case of Al-graphene nanocomposite). It is found that graphene inclusions strengthen metal-graphene nanocomposites. This is well consistent with experimental data reported in literature. Also, it is revealed that graphene inclusions in metal-graphene nanocomposites either hamper or enhance unstable GB migration and thereby grain growth driven by stress, depending on inclusion length. It is shown that shear-coupling effect provides more pronounced strengthening of nanocomposite and additional hampering of unstable GB migration compared to normal migration without a coupling shear.

1. INTRODUCTION

Nanostructured materials exhibit the excellent mechanical properties due to their specific structural features including ultra-small grain sizes and very large quantities of grain boundaries (GBs); see, e.g., [1-10]. As a corollary, GB-assisted and -mediated deformation micromechanisms can effectively contribute to plastic flow in these materials. Among such micromechanisms, of particular interest is the stress-driven GB migration that serves not only as a plastic deformation mode, but also as a mechanism of grain growth [11-30]. As a result, operation of stress-driven GB migration can modify material properties sensitive to grain size. Recently, a rapidly growing interest has been devoted to metal-matrix nanocomposites with nanoinclusions of graphene – a 2D carbon material with the unique mechanical properties [31-33] – being utilized as reinforcing fillers; see, e.g., [34-45]. These metal-graphene nanocomposites typically have metal matrices and demonstrate the outstanding mechanical characteristics such as high strength and Young modulus. Graphene nanoinclusions enhance strength of such nanocomposites owing to the three key factors: first, nanoinclusions act as obstacles to lattice dislocations movement; second, the stress transfer from a soft metal matrix to superstrong graphene nanofillers occurs; and, third, graphene

Corresponding author: S.V. Bobylev, e-mail: bobylev.s@gmail.com

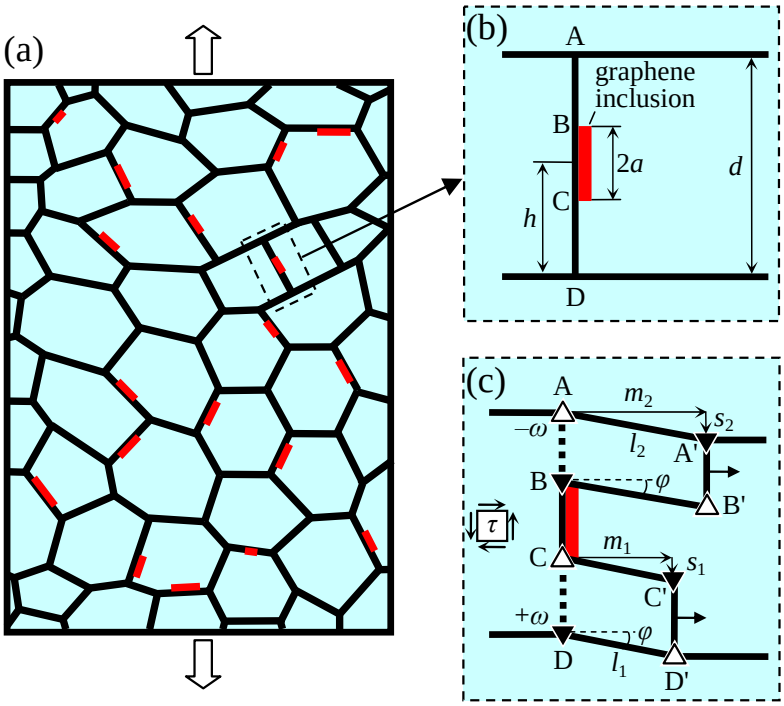

Fig. 1. Stress-driven shear-coupled migration of high-angle grain boundary in metal-graphene nanocomposite (schematically). (a) Nanostructured metal-matrix nanocomposite containing graphene nanoinclusions (red elongated rectangles) at grain boundaries (two-dimensional general view). (b) Nanocomposite fragment contains high-angle symmetric tilt boundary AD. Graphene nanoinclusion (red elongated rectangle) is located at this grain boundary. (c) Grain boundary AD migrates under stress to a new position A'B'BCC'D'. The shear-coupled migration process gives rise to the formation of two skewed disclination quadrupoles AA'B'B and CC'D'D (for details, see text).

nanoinclusions hamper both GB migration and thereby grain growth in nanocomposites during their synthesis involving mechanical and thermal treatment [38]. Micromechanism(s) and characteristics of hampering effects exerted by graphene nanoinclusions on GB migration are largely unknown. At the same time, their knowledge is of crucial importance for control and design of grain size in metal-graphene nanocomposites and thereby for enhancement in strength exhibited by such nanocomposites. Of utmost interest are the specific features of stress-driven GB migration in metal-graphene nanocomposites having nanostructured metal matrices; see, e.g., [46,47].

Earlier we proposed a model [47] describing plastic flow through stress-driven migration of high-angle GB in metal-graphene nanocomposites. Results of the model [47] provided important insight into the mechanics of plastic flow mediated by GB migration in metal-graphene nanocomposites, but that model does not take into account an important factor – shear coupling. In reality GB migration is often coupled with shear meaning that migration in the direction normal to GB plane is accompanied by tangential translation (parallel to GB plane) producing shear deformation of the lattice traversed by GB as shown in many molecular dynamics and quasi-continuum studies [15,48-54] as well as in experiments [11,55-61].

The main aim of this paper is to further elaborate theoretical description of stress-driven GB migration developed in our previous works [46,47] in metal-graphene nanocomposites to account for the effect of shear coupling. In doing so, we will theoretically examine stress-driven shear-coupled GB migration in metal-graphene nanocomposites using disclination theory.

2. STRESS-DRIVEN SHEAR-COUPLED MIGRATION OF GRAIN BOUNDARIES IN METAL-GRAPHENE NANOCOMPOSITES: GEOMETRIC ASPECTS

Graphene nanoinclusions are typically located at GBs of metal matrices in metal-graphene nanocomposites; see review [38] and references

therein. Let us consider a two-dimensional model of a metal-graphene nanocomposite specimen which is under tensile stress plastic flow (Fig. 1). In the framework of our model, plastic deformation involves stress-driven migration of the GB AD at which the graphene nanoinclusion is located (Figs. 1b and 1c). The GB AD is assumed to be a symmetric high-angle tilt boundary characterized by tilt misorientation angle θ. The graphene nanoinclusion represents a few-layer graphene nanoplatelet that has thickness of 1-2 nm (a red rectangle in Fig. 1) and is located at the fragment BC of the GB AD, as shown in Fig. 1b. When the shear stress τ is applied, the GB AD can migrate and thus mediate plastic flow.

In general, GB migration in a metal occurs through atomic rearrangements at the GB and in its vicinities in adjacent grain interiors. Such rearrangements are suppressed by immobile graphene nanoinclusions – metal atoms cannot move across graphene nanoplatelets – which thereby hamper the migration process. In this case, stress-driven migration of the GB AD hampered by the graphene nanoinclusion occurs as schematically shown in Figs. 1b and 1c. As to details, in the framework of our model, the segment BC of the GB AD is immobile (due to the presence of the immobile graphene nanoplatelet), whereas the GB segments AB and CD migrate to their new positions A'B' and C'D', respectively (Fig. 1c). In case of shear-coupled migration normal GB translation distances m_1 and m_2 (see Fig. 1c) of these segments are accompanied by tangential translations (shears) s_1 and s_2 in perpendicular direction (parallel to GB plane). A coupling factor β is introduced to define the ratio of shear to normal migration distance: $\beta = s_1/m_1 = s_2/m_2 = \tan\varphi$ (angle φ is shown in Fig. 1c). Coupling factor is defined by the atomic structure of a particular GB. Also, for convenience, we introduce migration distances l_1 and l_2 (Fig. 1c) accounting for both normal and tangential translation distances.

We now specify other geometric parameters of the system under consideration (see Fig. 1b). Let $2a$ be the length of graphene nanoinclusion (and the GB fragment BC), h denotes the distance between point D and middle point of the nanoinclusion, and d is the length of the GB AD (approximately equal to the grain size).

Stress-driven migration of the high-angle GB AD gives rise to the formation of new GB fragments BB' and CC' (Fig. 1b). Besides, for geometric reasons, stress-driven GB migration is accompanied by formation of wedge disclinations at GB junctions [62]. Let us examine this aspect in detail. In the case under consideration, we assume that GB junctions A and D in the initial state of the system (Fig. 1b) are geometrically compensated. That is, each of these junctions is characterized by the zero sum of misorientation angles specifying GBs adjacent to the junction; for details, see [62]. This, in particular, means that GB junctions do not create intermediate- and long-range stresses.

Stress-driven migration of the GB AD (Figs. 1b and 1c) violates balance of GB misorientation angles at pre-existent and new GB junctions A, B, C, D, A', B', C', and D' so that these junctions contain wedge disclinations (shown as triangles in Fig. 1c) serving as powerful stress sources. More precisely, two skewed disclination quadrupoles AA'B'B and CC'D'D (not rectangular like normal quadrupoles in case without shear coupling) are formed that consist of disclinations having strengths $\pm\omega$, where the strength magnitude ω is equal to tilt misorientation θ of the GB AD. Thus, all the disclinations shown in Fig. 1c have the same strength magnitude ω: disclinations with positive and negative strengths are shown as full and open triangles, respectively.

3. STRESS-DRIVEN SHEAR-COUPLED MIGRATION OF GRAIN BOUNDARIES IN METAL-GRAPHENE NANOCOMPOSITES: ENERGY AND STRESS CHARACTERISTICS

We now examine energy and stress characteristics of stress-driven shear-coupled GB migration in metal-graphene nanocomposites (Fig. 1). First, let us calculate the energy change ΔW that characterizes the migration transformation presented in Figs. 1b and 1c. Since defects are absent in the initial state of the system (Fig. 1b), the energy change ΔW comprised following five terms:

$$\Delta W = W_{AA'B'B} + W_{CC'D'D} + W_{int} + \Delta W_{gb} - A_{pl}. \qquad (1)$$

Here $W_{AA'B'B}$ and $W_{CC'D'D}$ are the proper energies of the skewed disclination quadrupoles AA'B'B and CC'D'D, respectively; W_{int} is the energy that specifies the elastic interaction between skewed disclination quadrupoles; ΔW_{gb} is the change in the GB energy due to the formation of the new GB segments BB' and CC'; and A_{pl} is the plastic deformation work.

The first three terms on the right-hand side of formula (1) are given by the expressions well known in the theory of disclinations in solids [62]. With these expressions, after some algebra, we have:

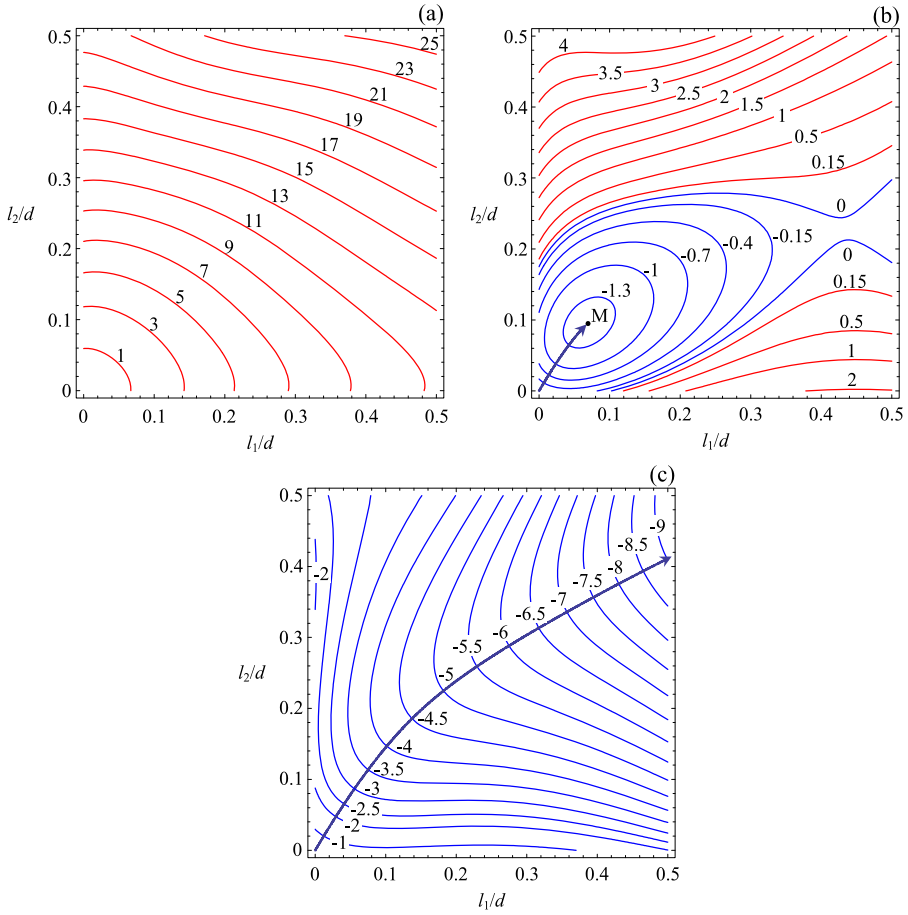

Fig. 2. The energy change ΔW dependences on the migration distances l_1 and l_2 in Al-graphene nanocomposite, for d = 50 nm, ω = 0.5, h = 0.4d, a = 0.1d, β = 0.5 and various values of the applied shear stress: (a) τ = 0.01$D\omega$, (b) τ = 0.7$D\omega$, and (c) τ = $D\omega$. The energy change levels are shown in units of $10^{-2}D\omega^2d^2$ near the corresponding contour lines.

$$
\begin{aligned}
W_{AA'B'B} + W_{CC'D'D} + W_{int} = \frac{D\omega^2}{4}\big[&f(L(p_1,l_1)) + f(L(p_1,-l_1)) - 2f(p_1) - 2f(l_1) + f(L(p_2,l_2))\\
&+f(L(p_2,-l_2)) - 2f(p_2) - 2f(l_2) + f(p_2+\delta) - f(\delta) - f(d) + f(p_1+\delta) + f(L(d,l_1))\\
&-f(L(p_1+\delta,l_1)) - f(L(p_2+\delta,l_1)) + f(L(\delta,l_1)) - f(L(p_2+\delta,-l_2)) + f(L(\delta,-l_2)) + f(L(d,-l_2))\\
&-f(L(p_1+\delta,-l_2)) - f(L(d,l_1-l_2)) + f(L(p_1+\delta,l_1-l_2)) + f(L(p_2+\delta,l_1-l_2)) - f(L(\delta,l_1-l_2))\big].
\end{aligned}
\tag{2}
$$

Here, for brevity, following notations are introduced: $D = G/[2\pi(1-\nu)]$, $f(x) = x^2\ln x^2$, $L(x,l) = \sqrt{x^2 + 2lx\sin\varphi + l^2}$, $p_1 = h - a$, $p_2 = d - h - a$, $\delta = 2a$, G is the shear modulus, and ν is the Poisson's ratio. The change in the GB energy due to the formation of the new GB segments BB' and CC' is evidently related to their sum length $l_1 + l_2$ as follows:

$$\Delta W_{gb} = \gamma\left(l_1 + l_2\right), \tag{3}$$

where γ is the specific (per unit area) surface energy of the GB. The work A_{pl} spent by the applied shear stress τ on movement of the GB fragments AB and CD over the migration distances l_1 and l_2, respectively (Fig. 1c), is given as:

$$A_{pl} = \tau\omega\left[l_1\left(h-a\right) + l_2\left(d-h-a\right)\right]. \tag{4}$$

Formulas (1)–(4) allow us to calculate the energy change ΔW that characterizes stress-driven shear-coupled migration of the GB (Figs. 1b and 1c). In the limiting case φ = 0 (migration without shear coupling)

we should arrive to the expression obtained in our previous work [47]. We calculated ΔW in the exemplary case of aluminum(Al)-graphene nanocomposite with Al matrix specified by the following values of material parameters: G = 26.5 GPa, ν = 0.34 [63], and γ = 0.4 J/m^2 [64]. Note that, generally speaking, the specific energy of a high-angle GB depends on its misorientation. However, in many metals, including Al, the GB energy as a function of GB misorientation is approximately constant, except for narrow ranges of misorientation angles at and near angles corresponding to special GBs [65]. As a corollary, our approximation of constant γ = 0.4 J/m^2 is good enough.

Fig. 2 demonstrates typical dependences $\Delta W(l_1,l_2)$ in the form of contour plots (2D maps) calculated for d = 50 nm, ω = 0.5, h = 0.4d, a = 0.1d, β = 0.5 and various values of the applied shear stress $\tau/(D\omega)$ = 0.01, 0.7, 1 (Figs. 2a, 2b, 2c, respectively). It is seen that, for low values of the applied stress (Fig. 2a), the energy change $\Delta W(l_1,l_2)$ monotonously grows with rising l_1 and/or l_2, that is, stress-driven shear-coupled GB migration is energetically unfavorable. For intermediate values of τ a local minimum (point M in Fig. 2b) appears at the map $\Delta W(l_1,l_2)$. It means that stress-driven migration of GB segments AB and CD over some limited (equilibrium) distances becomes energetically permitted. Evolution of the system towards equilibrium configuration is shown with the arrow in Fig. 2b. The local energy minimum corresponds to the equilibrium migration distances l_{e1} and l_{e2}. For high stresses, the energy change $\Delta W(l_1,l_2)$ monotonously decreases with rising l_1 and/or l_2 (Fig. 2c), meaning that stress-driven GB migration is unstable. It occurs as an energetically favorable process until at least one of the migrating GB segments AB or CD, is stopped at some structural obstacle, say, another GB.

The energy maps specifying Al have a character typical for almost any other fcc metal. In our earlier work [47] (regarding GB migration not coupled with shear) we have shown that behavior of Al- and Ni-based composites is almost identical and generally depends on the ratio γ/D, which is approximately the same for majority of fcc metals. So in this work, for shortness, we present results only for Al-graphene nanocomposites, which are representative of most fcc metal-graphene nanocomposites.

Using numerical analysis of the energy maps $\Delta W(l_1,l_2)$, we obtained dependences of the equilibrium migration distances l_{e1} and l_{e2} on various parameters of the system examined for ω = 0.5, d = 50 nm and the following values of coupling factor: β = 0, 0.5, 1 (Figs. 3, 4, 5, respectively). Figs. 3a, 4a, and 5a demonstrate typical dependences of equilibrium migration distances l_{e1} and l_{e2} on applied shear stress τ. These dependences show growth of the migration distances with rising the applied stress and transition to the unstable migration regime at some critical values (τ_{c2}) of the stress. The dependences of l_{e1} and l_{e2} on the parameter h specifying spatial position of the graphene nanoinclusion are presented in Figs. 3b, 4b, and 5b (for various value of coupling factor β, see above). With these dependences, a longer GB segment migrates over

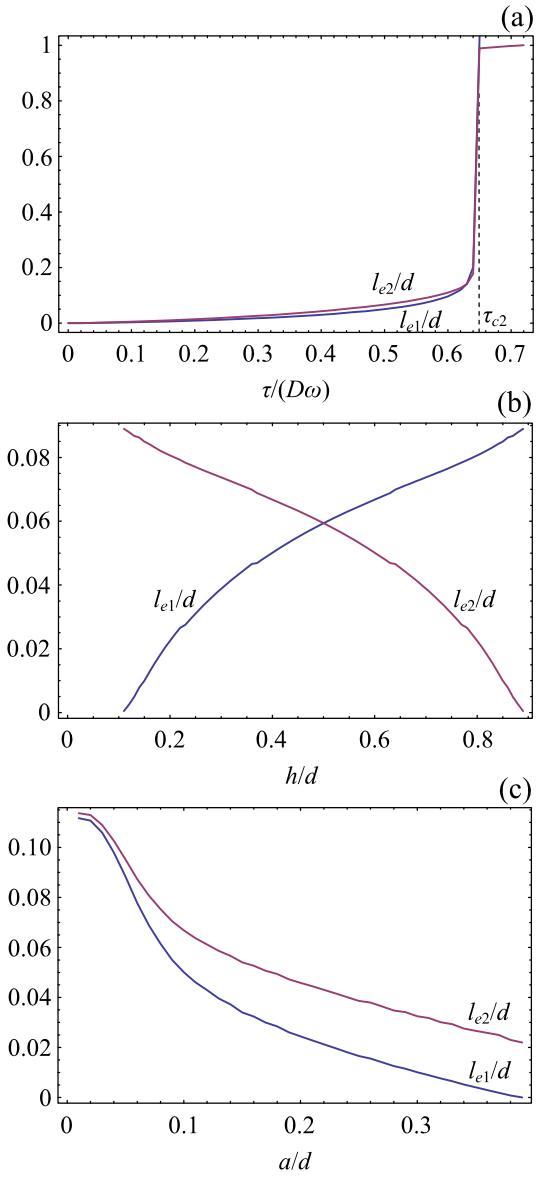

Fig. 3. Dependences of the equilibrium migration distances in Al-graphene nanocomposite, calculated at β = 0, d = 50 nm and ω = 0.5, on (a) the applied shear stress τ for h = 0.4d and a = 0.1d; (b) parameter h for τ = 0.5$D\omega$ and a = 0.1d; and (c) inclusion half-length a for τ = 0.5$D\omega$ and h = 0.4d.

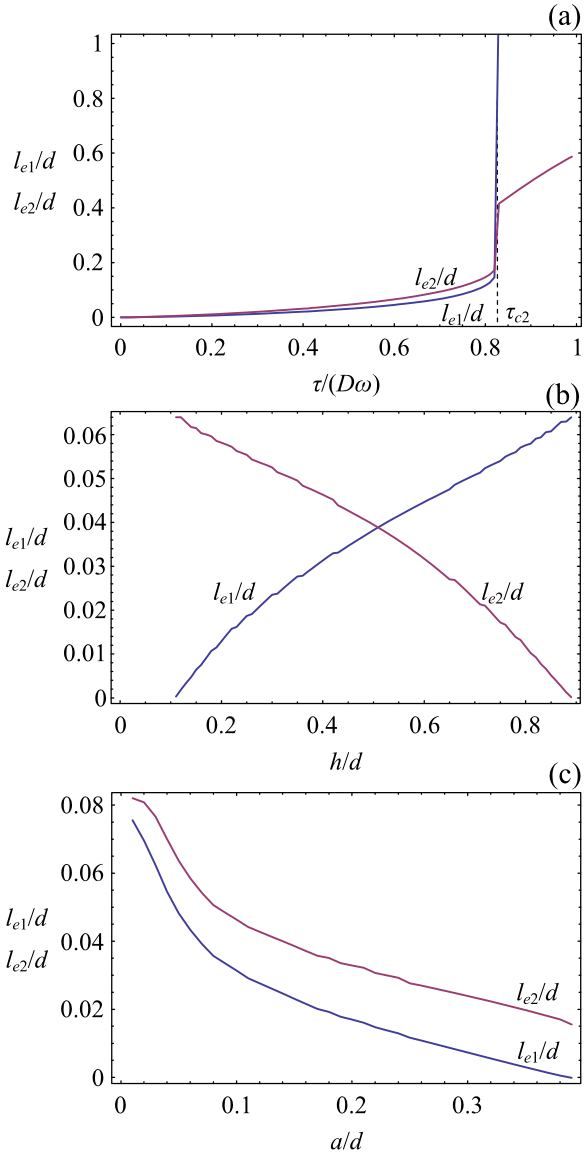

Fig. 4. Dependences of the equilibrium migration distances in Al-graphene nanocomposite, calculated at $\beta = 0.5$, $d = 50$ nm and $\omega = 0.5$, on (a) the applied shear stress τ for $h = 0.4d$ and $a = 0.1d$; (b) parameter h for $\tau = 0.5D\omega$ and $a = 0.1d$; and (c) inclusion half-length a for $\tau = 0.5D\omega$ and $h = 0.4d$.

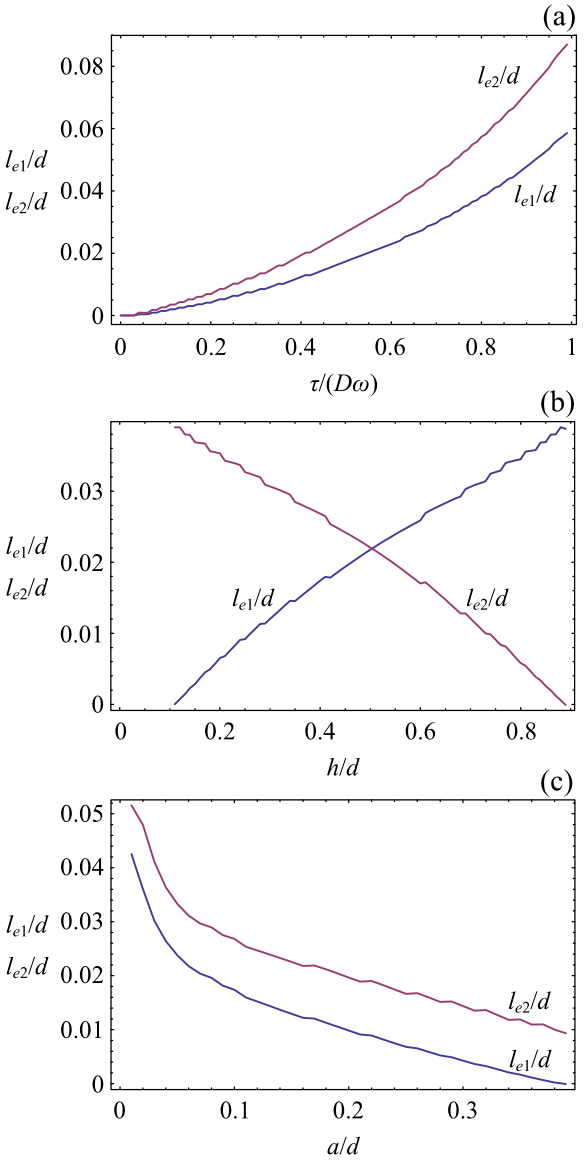

Fig. 5. Dependences of the equilibrium migration distances in Al-graphene nanocomposite, calculated for $\beta = 1$, $d = 50$ nm and $\omega = 0.5$, on (a) the applied shear stress τ for $h = 0.4d$ and $a = 0.1d$; (b) parameter h for $\tau = 0.5D\omega$ and $a = 0.1d$; and (c) inclusion half-length a for $\tau = 0.5D\omega$ and $h = 0.4d$.

a larger distance, as compared to a shorter GB fragment. In the partial case where the nanoinclusion is located exactly at the GB AD center, the migration distances l_{e1} and l_{e2} are identical. Figs. 3c, 4c, and 5c show dependences of l_{e1} and l_{e2} on the half-length a of the graphene nanoinclusion. From these figures it follows that the migration distances decrease when a increases. That is, longer inclusions more effectively hamper stress-driven GB migration than their shorter counterparts.

Comparison of the dependences presented in Figs. 3, 4 and 5 shows that for GBs characterized by higher value of coupling factor β equilibrium migration distances are considerably lower, that is, migration is suppressed for those boundaries. This is also means that for GB characterized by relatively high value of β transition into unstable migration regime might be not possible at all (under realistic values of applied stress), which is clearly seen from Figs. 3a, 4a, and 5a.

Let us introduce the critical stresses τ_{c1} and τ_{c2} for the migration onset and transition to the unstable migration regime, respectively. These stresses serve as important characteristics of stress-driven GB migration. The critical stress τ_{c1} is defined as the minimum stress at which the migration onset is energetically favorable. More precisely, τ_{c1} is defined as the minimum stress at which one of the equilibrium migration distances (l_{e1} or l_{e2}) achieves some characteristic minimum value (denoted as b) allowing one to identify the fact experimentally that GB migrates. We take b as a GB width, that is, as a good approximation we have: b = 1 nm. After numerical analysis of the calculated dependences (Figs. 3–5), we find typical values of τ_{c1}. For instance, in Al-graphene nanocomposites with ω = 0.5, a = 0.1d, h = 0.4d, d = 50 nm and various values of coupling factor β = 0, 0.5, and 1, we obtain: $\tau_{c1} \approx$ 830, 960, and 1310 MPa, respectively. Thus, values of the critical stress τ_{c1} for the migration onset in metal-graphene nanocomposites are larger for GBs characterized by higher values of coupling factor. Also, the result obtained in our earlier model [47] is still valid: critical stresses for the migration onset in metal-graphene nanocomposites are significantly larger than those stresses in unreinforced (pure) metals. At the same time, values of the critical stress τ_{c1} are rather realistic. They can be achieved in conventional quasistatic deformation regimes so that stress-driven GB migration can effectively contribute to plastic flow in metal-graphene nanocomposites. If it is so, with comparatively high values of the critical stress τ_{c1}, one concludes that graphene nanoinclusions make metal-graphene nanocomposites stronger as compared to pure metals. This theoretical conclusion is well consistent with experimental data reported in the literature; see review [38] and references therein.

We now numerically estimate the critical stress τ_{c2} specifying transition to the unstable migration regime. Estimation results are presented in Figs. 6–8. In particular, Fig. 6 demonstrates dependences of $\tau_{c2}(a)$ for ω = 0.5, h/d = 0.2, 0.3, 0.4, 0.5 (these values are shown near the corresponding curves), d = 50 nm and various values of coupling factor β = 0, 0.5, and 1 (Figs. 6a, 6b, and 6c, respectively). Dashed lines in these figures show the values of the critical stress τ'_{c2} for the unstable migration in pure metal (without inclusions). To calculate the latter stress in the case of β = 0 we used the results of the model [13] and for β > 0 we used the results of this work in the limiting case ($a \to 0$) and manually assigning ΔW_{gb} = 0. In doing so, we get for β = 0, 0.5, and 1: τ'_{c2} = 0.8$D\omega$, 1.05 $D\omega$, and 1.65 $D\omega$, respectively. As it follows from Fig. 6 (and also Figs. 7 and 8), the inequality $\tau_{c2} < \tau'_{c2}$ holds in a wide range of nanoinclusion sizes (a < 0.2 – 0.3d, depending on parameter h). That is, transition to the unstable migration in metal-graphene nanocomposites is enhanced as compared to that in pure metals, which is somewhat surprising considering that the first critical stress τ_{c1} is always higher in nanocomposites than in pure metal (see above). From a physical viewpoint, this is related to

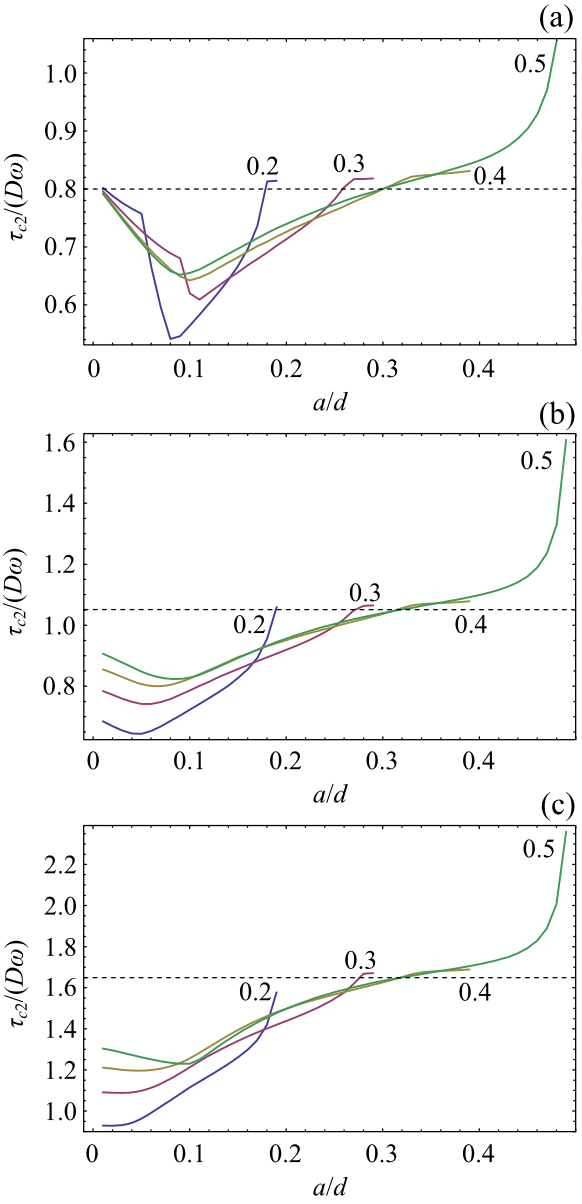

Fig. 6. Dependences of the critical shear stress τ_{c2} in Al-graphene nanocomposite on inclusion half-length a, calculated for various values of parameter h (these values are shown in units of d near corresponding curves), ω = 0.5, d = 50 nm and (a) β = 0; (b) β = 0.5; (c) β = 1.

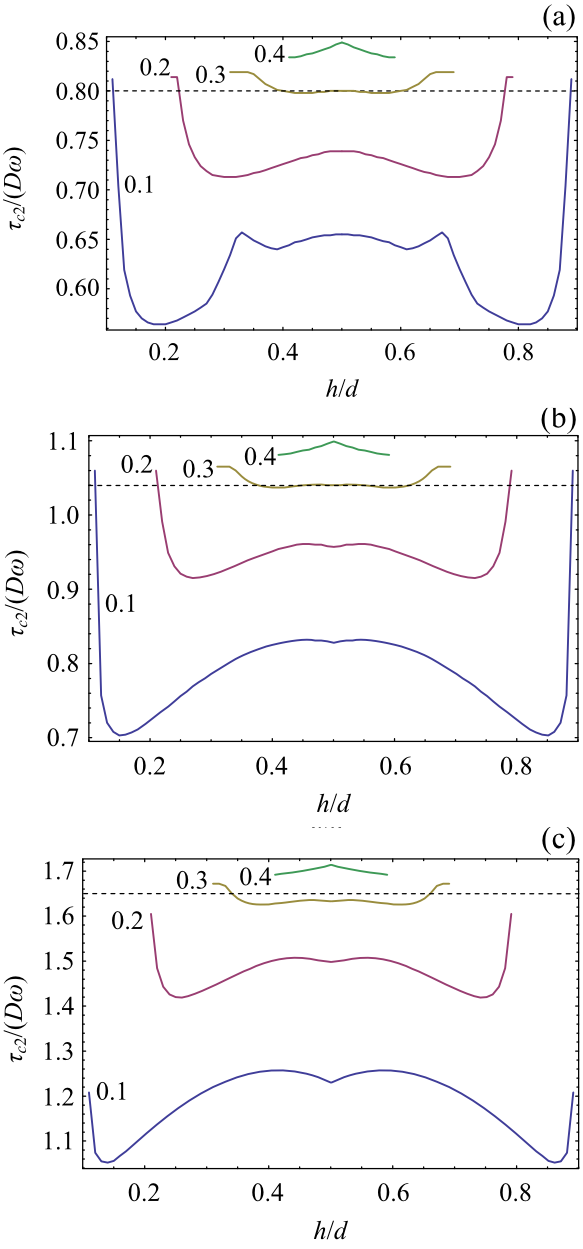

Fig. 7. Dependences of the critical shear stress τ_{c2} in Al-graphene nanocomposite on parameter h, calculated for various values of inclusion half-length a (these values are shown in units of d near corresponding curves), $\omega = 0.5$, $d = 50$ nm and (a) $\beta = 0$; (b) $\beta = 0.5$; (c) $\beta = 1$.

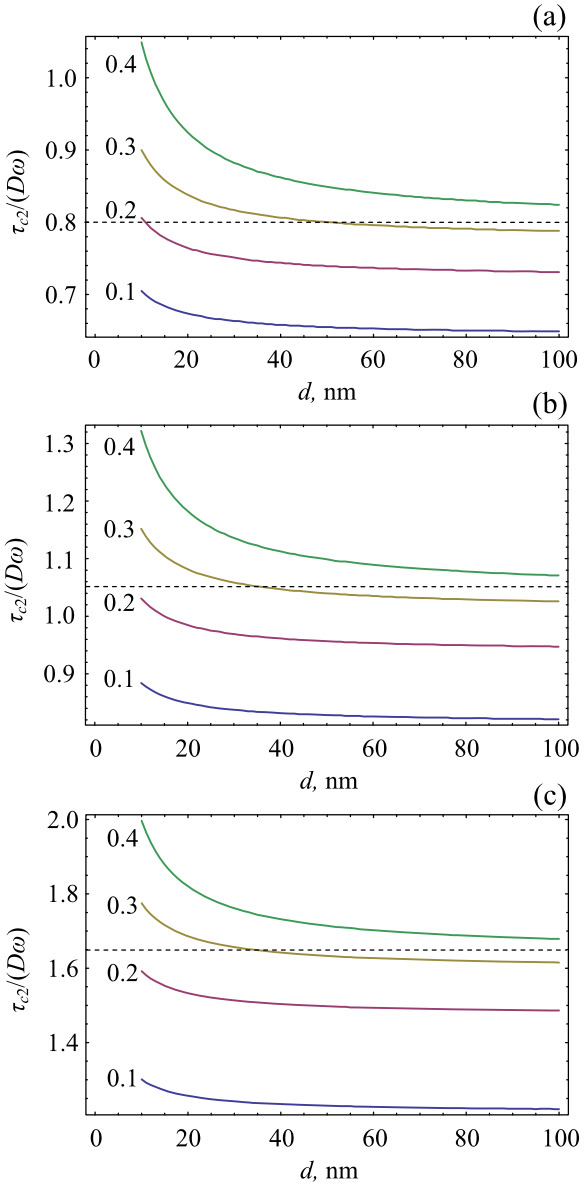

Fig. 8. Dependences of the critical shear stress τ_{c2} in Al-graphene nanocomposite GB length (approximately equal to grain size) d, calculated for various values of inclusion half-length a (these values are shown in units of d near corresponding curves), $\omega = 0.5$, $h = 0.5d$ and (a) $\beta = 0$; (b) $\beta = 0.5$; (c) $\beta = 1$.

the fact that the defect configuration shown in Fig. 1c in the discussed range of nanoinclusion lengths due to the effective mutual screening of stress fields created by the disclination quadrupoles AA'B'B and CC'D'D has lower energy than configuration without inclusion (similar to one examined in the model [13] in the case of unreinforced metals).

Also, note (see Fig. 6) that dependences $\tau_{c2}(a)$ generally have pronounced minimum in the range $a \leq 0.1d$ (exact value of a depends on the coupling factor). That is, GBs with graphene nanoinclusions specified by these values of a show the tendency to easily migrate under stress and composites with those nanoinclusions must be prone to enhanced grain growth (which should generally be avoided).

Fig. 7 present dependences $\tau_{c2}(h)$ calculated for $\omega = 0.5$, $a/d = 0.1$, 0.2, 0.3, 0.4 (these values are shown near the corresponding curves), $d = 50$ nm and various values of coupling factor $\beta = 0$, 0.5, and 1 (Figs. 7a, 7b, and 7c, respectively). It is seen that dependences $\tau_{c2}(h)$ are significantly sensitive to the

graphene nanoplatelet length. Indeed, for comparatively short nanoinclusions, the dependences $\tau_{c2}(h)$ have complex character with several local minimums (from 2 to 4 depending on values of a and coupling factor β); see curves corresponding to values a/d = 0.1, 0.2, 0.3 in Fig. 7. For comparatively long nanoinclusions (see curves with a/d = 0.4) we have quite the different character: the dependences $\tau_{c2}(h)$ do not have minimums and instead have maximum at h = 0.5. Using dependences $\tau_{c2}(a)$ and $\tau_{c2}(h)$ presented in Figs. 6 and 7 we can easily identify "soft" configurations characterized by minimum values of τ_{c2} and, thus, displaying easier (occurring under lower applied stresses) grain growth.

General conclusion we get from the analysis above is that transition in unstable migration regime are mainly dependent on nanoinclusion length given by parameter $2a$. The unstable migration serves as the dominant mechanism for grain growth in mechanically treated metals. In this context, our theoretical analysis shows that grain growth is enhanced in plastically deformed metal-graphene nanocomposites with relatively "short" graphene nanoplatelets specified by lengths $2a < 0.4 – 0.6d$, as compared to pure metals. At the same time, in the case of "long" graphene nanoinclusions with $2a > 0.4 – 0.6d$, the critical stress for the unstable migration satisfy the inequality $\tau_{c2} > \tau'_{c2}$ so that grain growth is hampered in metal-graphene nanocomposites as compared to pure metal.

Fig. 8 presents dependences $\tau_{c2}(d)$ calculated for ω = 0.5, h = 0.5, a/d = 0.1, 0.2, 0.3, 0.4 (these values are shown near the corresponding curves) and various values of coupling factor β = 0, 0.5, and 1 (Figs. 8a, 8b, and 8c, respectively). It is seen that critical stress τ_{c2} significantly grows with decreasing grain size. Thus, in nanocomposites characterized by extremely small grain sizes, the unstable migration is hampered (compared to pure metals) in all range of nanoinclusion parameters.

Comparison of plots presented in Figs. 6–8 corresponding to different values of coupling factor β shows that critical stress τ_{c2} is higher for GBs characterized by higher values of β in all range of parameters, so unstable migration is hampered for such GBs. The reason for this hampering is fairly obvious: shear-coupled migration gives rise to the formation of skewed disclination quadrupoles that have much higher elastic energy than normal (rectangular) quadrupoles formed in case of the migration uncoupled with shear [46,47]. It means that in our previous model [47], where shear coupling was not accounted for, critical stresses for both migration onset and unstable migration were underestimated.

To summarize the obtained results, we may conclude that stress-driven shear-coupled GB migration in metal-graphene nanocomposites is either enhanced or hampered (compared to unhindered migration in pure metals) by graphene nanoinclusions, depending on their typical length and GB length (grain size). At the same time the effect of shear coupling always leads to the increase in critical stresses for both migration onset and unstable migration.

4. CONCLUDING REMARKS

Thus, we theoretically described stress-driven shear-coupled GB migration in metal-graphene nanocomposites. In the framework of our description, stress-driven shear-coupled migration of high-angle GBs gives rise to the formation of both new GB fragments and wedge disclinations at GB junctions and edges of graphene inclusions. The new GB fragments and disclinations cause the main hampering force for the migration process.

Energy and stress characteristics of stress-driven shear-coupled GB migration in metal-graphene nanocomposites are calculated. In particular, we revealed that the critical stress τ_{c1} for the migration onset in metal-graphene nanocomposites is significantly larger than its counterpart τ'_{c1} in unreinforced metals. Accounting for shear coupling effect increase this critical stress even more compared to the case of GB migration uncoupled with shear [47]. At the same time, values of the critical stress τ_{c1} are rather realistic. They can be achieved in conventional quasistatic deformation regimes so that stress-driven shear-coupled GB migration can effectively contribute to plastic flow in metal-graphene nanocomposites. If it is so, with comparatively high values of the critical stress τ_{c1}, one concludes that graphene nanoinclusions make metal-graphene nanocomposites stronger as compared to pure metal. This theoretical conclusion is well consistent with experimental data reported in literature (for a review, see [38]).

Also, it is revealed that stress-driven grain growth in metal-graphene nanocomposites is either enhanced or hampered by graphene nanoinclusions, when they are long or short, respectively. These results are of great interest for synthesis of metal-graphene nanomposites with controlled microstructure and enhanced strength. In particular, fabrication of metal-matrix nanocomposites containing

"long" graphene nanoinclusions will allow one to stabilize grain size in metal matrix and thus control its strength contributing to strength characteristics of nanocomposites.

ACKNOWLEDGEMENTS

This work was supported by the Council for grants of the President of Russian Federation (grant MD-3154.2017.1) and by the Russian Ministry of Education and Science (Zadanie 16.3483.2017/PCh).

REFERENCES

[1] C.C. Koch, I.A. Ovid'ko, S. Seal and S. Veprek, *Structural Nanocrystalline Materials: Fundamentals and Applications* (Cambridge University Press, Cambridge, 2007).
[2] M. Dao, L. Lu, R.J. Asaro, J.T.M. De Hosson and E. Ma // *Acta. Mater*. **55** (2007) 4041.
[3] E.C. Aifantis // *Mater. Sci. Eng. A* **503** (2009) 190.
[4] J.R. Greer and J.T.M. De Hosson // *Prog. Mater. Sci*. **56** (2011) 654.
[5] I.A. Ovid'ko and T.G. Langdon // *Rev. Adv. Mater. Sci.* **30** (2012) 103.
[6] Y.T. Zhu, X.Z. Liao and X.L. Wu // *Prog. Mater. Sci.* **57** (2012) 1.
[7] R.Z. Valiev, A.P. Zhilyaev and T.G. Langdon, *Bulk Nanostructured Materials: Fundamentals and Applications* (Wiley, Hoboken, New Jersey, USA, 2014).
[8] R.Z. Valiev and Y.T. Zhu // *Trans. MRS Japan* **40** (2015) 309.
[9] M. Kawasaki and T.G. Langdon // *J. Mater. Sci.* **51** (2016) 19.
[10] P. Kumar, M. Kawasaki and T.G. Langdon // *J. Mater. Sci.* **51** (2016) 7.
[11] M. Jin, A.M. Minor, E.A. Stach and J.W. Morris // *Acta. Mater*. **52** (2004) 5381.
[12] W.A. Soer, J.T.M. De Hosson, A.M. Minor, J.W. Morris and E.A. Stach // *Acta. Mater.* **52** (2004) 5783.
[13] M.Yu. Gutkin and I.A. Ovid'ko // *Appl. Phys. Lett.* **87** (2005) 251916.
[14] J.T.M. De Hosson, W.A. Soer, A.M. Minor, Z.W. Shan, E.A. Stach, S.A. Syed Asif and O.L. Warren // *J. Mater. Sci.* **41** (2006) 7704.
[15] D. Farkas, A. Frřseth and H. Van Swygenhoven // *Scr. Mater.* **55** (2006) 695.
[16] D.S. Gianola, S. Van Petegem, M. Legros, S. Brandstetter, H. Van Swygenhoven and K.J. Hemker // *Acta. Mater*. **54** (2006) 2253.
[17] D.S. Gianola, D.H. Warner, J.F. Molinari and K.J. Hemker // *Scr. Mater.* **55** (2006) 649.
[18] X.Z. Liao, A.R. Kilmametov, R.Z. Valiev, H.S. Gao, X.D. Li, A.K. Mukherjee, J.F. Bingert and Y.T. Zhu // *Appl. Phys. Lett*. **88** (2006) 021909.
[19] F. Sansoz and V. Dupont // *Appl. Phys. Lett*. **89** (2006) 111901.
[20] V. Dupont and F. Sansoz // Acta. Mater. 56 (2008) 6013.
[21] I.A. Ovid'ko, A.G. Sheinerman and E.C. Aifantis // *Acta. Mater.* **56** (2008) 2718.
[22] S.V. Bobylev, N.F. Morozov and I.A. Ovid'ko // *Phys. Rev. Lett.* **105** (2010) 055504.
[23] S.V. Bobylev, N.F. Morozov and I.A. Ovid'ko // *Phys. Rev. B* **84** (2011) 094103.
[24] J.A. Sharon, P.-C. Su, F.B. Prinz and K.J. Hemker // *Scr. Mater*. **64** (2011) 25.
[25] S.V. Bobylev and I.A. Ovid'ko // *Phys. Rev. Lett.* **109** (2012) 175501.
[26] S.V. Bobylev and I.A. Ovid'ko // *Acta. Mater*. **88** (2015) 260.
[27] Y.J. Lin, H.M. Wen, Y. Li, B. Wen, W. Liu and E.J. Lavernia // *Acta. Mater*. **82** (2015) 304.
[28] I.A. Ovid'ko and A.G. Sheinerman // *J. Mater. Sci.* **50** (2015) 4430.
[29] I.A. Ovid'ko and A.G. Sheinerman // *Acta. Mater*. **121** (2016) 117.
[30] S.V. Bobylev and I.A. Ovid'ko // *Acta. Mater*. **124** (2017) 333.
[31] C. Lee, X.D. Wei, J.W. Kysar and J. Hone // *Science* **321** (2008) 385.
[32] I.A. Ovid'ko // *Rev. Adv. Mater. Sci.* **34** (2013) 1.
[33] C. Daniels, A. Horning, A. Phillips, D.V. Massote, L. Liang, Z. Bullard, B.G. Sumpter and V. Meunier // *J. Phys.: Condens. Matter* **27** (2015) 373002.
[34] J. Hwang, T. Yoon, S.H. Jin, J. Lee, T.S. Kim, S.H. Hong and S. Jeon // *Adv. Mater.* **25** (2013) 6724.
[35] Y. Kim, J. Lee, M.S. Yeom, J.W. Shin, H. Kim, Y. Cui, J.W. Kysar, J. Hone, Y. Jung, S. Jeon and S.M. Han // *Nat. Commun.* **4** (2013) 2114.
[36] D. Kuang, L.Y. Xu, L. Liu, W.B. Hu and Y.T. Wu // *Appl. Surf. Sci*. **273** (2013) 484.
[37] A.G. Nasibulin, T. Koltsova, L.I. Nasibulina, I.V. Anoshkin, A. Semencha, O.V. Tolochko and E.I. Kauppinen // *Acta. Mater.* **61** (2013) 1862.
[38] I.A. Ovid'ko // *Rev. Adv. Mater. Sci*. **38** (2014) 190.

[39] C.L.P. Pavithra, B.V. Sarada, K.V. Rajulapati, T.N. Rao and G. Sundararajan // *Sci. Rep.* **4** (2014).
[40] H. Algul, M. Tokur, S. Ozcan, M. Uysal, T. Cetinkaya, H. Akbulut and A. Alp // *Appl. Surf. Sci.* **359** (2015) 340.
[41] S.N. Alam and L. Kumar // *Mater. Sci. Eng. A* **667** (2016) 16.
[42] V.G. Konakov, O.Y. Kurapova, I.V. Lomakin, I.Y. Archakov, E.N. Solovyeva and I.A. Ovid'ko // *Rev. Adv. Mater. Sci*. **44** (2016) 361.
[43] D.D. Zhang and Z.J. Zhan // *J. Alloy Compd*. **654** (2016) 226.
[44] D.D. Zhang and Z.J. Zhan // *J. Alloy Compd*. **658** (2016) 663.
[45] O.Y. Kurapova, V.G. Konakov, A.S. Graschenko, N.N. Novik, S.N. Golubev and I.A. Ovid'ko // *Rev. Adv. Mater. Sci*. **48** (2017) 71.
[46] S.V. Bobylev, N.F. Morozov and I.A. Ovid'ko // *Dokl. Phys*. **62** (2017) 124.
[47] S.V. Bobylev, N.F. Morozov and I.A. Ovid'ko // *Rev. Adv. Mater. Sci.* **48** (2017) 131.
[48] D. Farkas, S. Mohanty and J. Monk // *Mater. Sci. Eng. A* **493** (2008) 33.
[49] N. Chandra and P. Dang // *J. Mater. Sci.* **34** (1999) 655.
[50] L. Wan and S. Wang // *Phys. Rev. B* **82** (2010) 214112.
[51] G.H. Bishop Jr., R.J. Harrison, T. Kwok and S. Yip // *J. Appl. Phys.* **53** (1982) 5596.
[52] G.H. Bishop Jr, R.J. Harrison, T. Kwok and S. Yip // *J. Appl. Phys*. **53** (1982) 5609.
[53] J.W. Cahn, Y. Mishin and A. Suzuki // *Acta. Mater*. **54** (2006) 4953.
[54] J.W. Cahn, Y. Mishin and A. Suzuki // *Philos. Mag.* **86** (2006) 3965.
[55] T. Gorkaya, T. Burlet, D.A. Molodov and G. Gottstein // *Scr. Mater.* **63** (2010) 633.
[56] T. Gorkaya, D.A. Molodov and G. Gottstein // *Acta. Mater.* **57** (2009) 5396.
[57] M. Legros, D.S. Gianola and K.J. Hemker // *Acta. Mater.* **56** (2008) 3380.
[58] F. Mompiou, D. Caillard and M. Legros // *Acta. Mater.* **57** (2009) 2198.
[59] F. Mompiou, M. Legros and D. Caillard // *J. Mater. Sci.* **46** (2011) 4308.
[60] A.D. Sheikh-Ali // *Acta. Mater.* **58** (2010) 6249.
[61] A.D. Sheikh-Ali and J.A. Szpunar // *Mater. Sci. Eng. A* **245** (1998) 49.
[62] A.E. Romanov and V.I. Vladimirov, In: *Dislocations in solids*, vol. 9, ed. by F.R.N. Nabarro (North Holland, Amsterdam, 1992), p. 191.
[63] J.P. Hirth and J. Lothe, *Theory of dislocations* (Wiley, New York, 1982).
[64] A.P. Sutton and R.W. Balluffi // *Acta Metall.* **35** (1987) 2177.
[65] A.P. Sutton and R.W. Ballufi, *Interfaces in crystalline materials* (Oxford University Press, Oxford, UK, 1995).